Clinical Research in Cardiology (2019) 108:1059–1068
https://doi.org/10.1007/s00392-019-01439-5

ORIGINAL PAPER

Qualitative and quantitative neointimal characterization by optical coherence tomography in patients presenting with in-stent restenosis

Erion Xhepa[1] · Robert A. Byrne[1] · Fernando Rivero[2] · Andi Rroku[1] · Javier Cuesta[2] · Gjin Ndrepepa[1] · Sebastian Kufner[1] · Teresa Bastante Valiente[2] · Salvatore Cassese[1] · Marcos Garcia-Guimaraes[2] · Anna Lena Lahmann[1] · Himanshu Rai[1] · Heribert Schunkert[1,4] · Michael Joner[1,4] · María José Pérez-Vizcayno[3] · Nieves Gonzalo[3] · Fernando Alfonso[2] · Adnan Kastrati[1,4]

Received: 13 January 2019 / Accepted: 13 February 2019 / Published online: 19 February 2019

Abstract

Aims To describe optical coherence tomography (OCT) findings in patients with in-stent restenosis (ISR) and determine predictors of neointimal patterns and neoatherosclerosis.

Methods and results Patients undergoing OCT prior to PCI for ISR in three European centres were included. Analyses were performed in a core laboratory. Qualitative and quantitative [gray-scale signal intensity (GSI)] neointima analyses were performed on a per quadrant basis. A total of 107 patients were included. Predominantly homogeneous lesions included 4.5% (0.0–14.3) non-homogeneous quadrants, while predominantly non-homogeneous ones included 28.1% (20.3–37.5) homogeneous quadrants. Mean GSI values differed significantly between homogeneous [108.4 (92.5–123.6)], non-homogeneous [79.9 (61.2–95.9)], and neoatherosclerosis [88.3 (72.8–104.9)] quadrants ($p < 0.001$ for all comparisons). Stent underexpansion was observed in 48.5% and 61.1% of lesions, respectively ($p = 0.225$). Female sex and maximal neointimal thickness independently correlate with a non-homogeneous pattern, while angiographic pattern and diabetes mellitus inversely correlate with such pattern. Time from index stenting procedure was the only independent predictor of neoatherosclerosis.

Conclusions Different neointimal patterns coexist in a significant proportion of ISR lesions. GSI values differ significantly between neointimal categories. Neoatherosclerosis is a time-dependent phenomenon, displaying different time courses in DES compared to BMS, with earlier appearance in the former group. Stent underexpansion is a frequent finding in patients with ISR.

Keywords Optical coherence tomography · In-stent restenosis · Neoatherosclerosis · Neointimal characterization · Gray-scale signal intensity analysis

Introduction

Constant improvements in safety and efficacy of percutaneous coronary interventions (PCI) have resulted in highly satisfactory outcomes in the majority of patients undergoing stent implantation. However, large real-world reports, including angiographic surveillance, have shown rates of angiographic in-stent restenosis (ISR) of 12–15%, depending on the generation of drug-eluting stent (DES) being used [1]. Therefore, a not negligible incidence of ISR coupled with increasing numbers and complexity of PCI worldwide [2], account for relevant numbers of patients presenting with such entity in absolute terms.

Based on its properties at optical coherence tomography (OCT) imaging, neointimal tissue has been subdivided in

Electronic supplementary material The online version of this article (https://doi.org/10.1007/s00392-019-01439-5) contains supplementary material, which is available to authorized users.

✉ Erion Xhepa
xhepa@dhm.mhn.de

1 Deutsches Herzzentrum München, Klinik an der Technischen Universität München, Munich, Germany

2 Hospital Universitario de La Princesa, Madrid, Spain

3 Hospital Universitario Clínico San Carlos, Madrid, Spain

4 DZHK (German Centre for Cardiovascular Research), Partner Site Munich Heart Alliance, Munich, Germany

three different patterns: (i) homogeneous, (ii) heterogeneous, and (iii) layered [3], which correlate with different histological substrates [4]. However, validation studies against the gold standard of histology remain relatively scarce. The largest post-mortem study to date showed homogeneous patterns to consistently correlate with abundance of smooth muscle cells embedded in collagen/proteoglycan rich tissue, while heterogeneous and layered patterns revealed a multitude of corresponding histological components [5]. In addition, histological studies have shown marked heterogeneity in vessel healing following stent implantation [6, 7]. Although previous studies have explored correlations between neointimal patterns, underlying stent type and restenosis phase [8–10], the degree of intralesion neointimal heterogeneity has not been systematically investigated.

We sought to perform an OCT based qualitative and quantitative neointimal characterization as well as define predictors of neointimal patterns and neoatherosclerosis (NA) in a large patient cohort undergoing PCI for ISR.

Methods

Study population and angiographic data analysis

Patients presenting with ischemic symptoms and/or evidence of myocardial ischemia in three European centers (Deutsches Herzzentrum, Munich, Germany; Hospital Universitario de La Princesa and Hospital Universitario Clínico San Carlos, Madrid, Spain) and undergoing intravascular OCT prior to PCI for ISR were included in this study. Baseline and post-procedural angiograms were recorded and assessed off-line in a core laboratory (ISAResearch Center, Munich, Germany) with an automated edge-detection system (Medis Medical Imaging Systems, Leiden, The Netherlands). The angiographic pattern of ISR was classified according to the Mehran's classification [11].

OCT data acquisition and morphometric analysis

Following administration of intracoronary nitrates, OCT was performed with non-occlusive technique using frequency-domain OCT imaging systems (C7XR, Illumien or Illumien Optis). Briefly, a rapid exchange imaging catheter (Dragonfly™ or Dragonfly Duo™) was advanced beyond the stented segment. An OCT pullback of the entire stented segment, including proximal and distal reference sites, was performed with contrast injection through the guiding catheter at 3–5 ml/s.

Raw data of OCT image acquisitions were sent to a centralized core laboratory (ISAResearch Center, Munich, Germany). Quantitative and morphometric analyses were performed every 1 mm along the entire stented segment. Dedicated software (St. Jude Medical, St. Paul, MN, USA) was used for quantification. Further details and definitions are provided in the Appendix in the online-only Data Supplement.

Qualitative neointimal characterization and gray-scale signal intensity analysis

Characterization of neointimal tissue was performed at the frame displaying the maximal %AS as well as the 5 preceding and following analyzed frames; in other words, a 10 mm segment was analyzed, given a %AS of at least 50% was present in each frame. Each frame was subdivided in four quadrants (90°) and the neointimal characteristics separately characterized for each of them. Based on its optical characteristics, neointimal tissue was categorized as homogeneous, heterogeneous, or layered. Atherosclerotic changes of the neointima were defined by the presence of one or more of the following: macrophage infiltration and/or lipid-laden tissue within the stent and neointimal calcification (Fig. 1a–i) [12]. To assess interobserver variability in neointimal characterization, a subgroup of 50 randomly chosen pullbacks were independently analyzed by 2 experienced cardiologists.

Quantitative analysis of the neointimal tissue by means of gray-scale signal intensity (GSI) analysis was performed on a per quadrant basis. We have previously shown that GSI analysis accurately differentiates between mature and immature neointimal tissue following coronary stenting [13, 14]. Analyses were performed using Image J software (free-ware available at https://imagej.nih.gov/ij/index.html) (Fig. 2). Further details are provided in the Appendix in the online-only Data Supplement.

Statistical analysis

Continuous data are presented as mean ± SD or median (25th–75th percentiles) depending on the distribution pattern of the variable. Categorical data are presented as frequencies or proportions (%). Differences between groups were assessed using the student's *t* test, Wilcoxon rank sum test, Kruskal–Wallis, or one-way analysis of variance for continuous variables and the Chi-square test (or Fischer's exact test, where the expected cell value was < 5) for categorical variables. Pairwise multiple comparisons were performed by means of the Tukey's test. To account for the clustered nature of the data, a generalized linear mixed model was conducted for the analysis of OCT data. The model contained a fixed-effects term (either neointimal type or stent type) and a random-effects term (patient for frame-level analysis, patient and frame for strut-level analysis). Predictors of neointimal pattern as well as of NA were assessed by means of multivariable

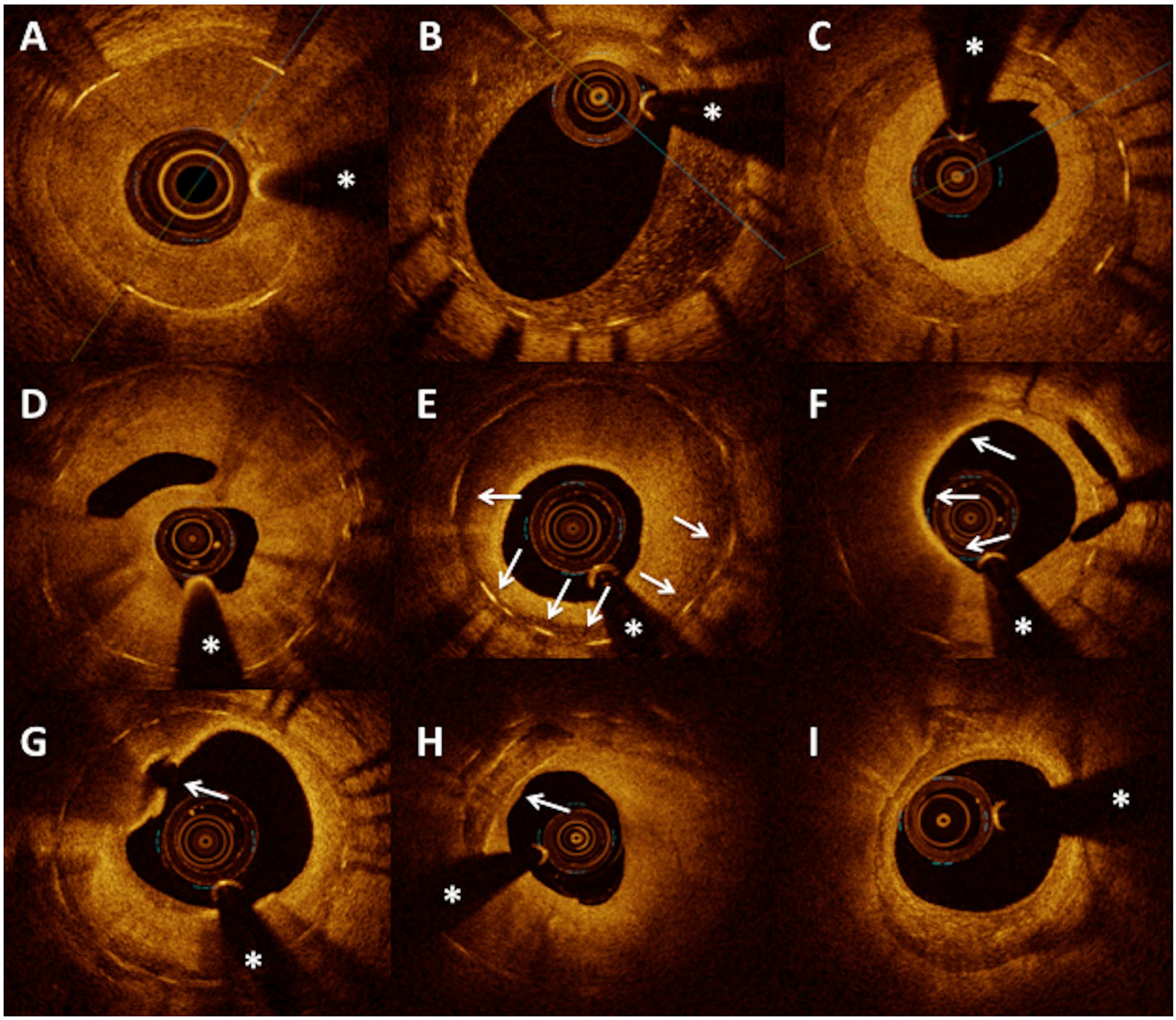

Fig. 1 Representative images of optical coherence tomography findings in patients presenting with in-stent restenosis. **a** In-stent restenosis with homogeneous neointimal pattern. **b** In-stent restenosis with heterogeneous neointimal pattern. **c** In-stent restenosis with a layered neointimal pattern. **d** Severe in-stent restenosis with a bridging architecture of the neointima. **e** Peri-strut low-intensity areas (arrows). **f** Macrophage infiltration involving a 180° neointimal arc (arrows from 6 to 12 o'clock). **g** Neoatherosclerosis and ruptured thin-cap fibroatheroma (arrow). **h** Neointimal calcification (arrow). **i** Severe concentric in-stent calcification and neoatherosclerosis obscuring underlying stent struts. *Guidewire artifact

analysis. The selection of variables for the multivariable model was performed using the LASSO regression method [15] after entering all relevant clinical, angiographic, and OCT parameters as candidates. The degree of agreement between reviewers was quantified using Cohen's κ test for concordance. All tests were two-sided and assessed at a significance level of 5%. The statistical analysis was performed by means of R software (version 3.5.1, R Foundation for Statistical Computing, Vienna, Austria) and SPSS Version 23 (IBM Corp, Armonk, New York).

Results

A total of 107 patients undergoing PCI for ISR between 2010 and 2015 were included, with one lesion being imaged/treated per patient; 73 lesions displayed a predominantly homogeneous and 34 lesions a predominantly non-homogeneous neointima. Baseline clinical and angiographic characteristics of the patient population are displayed in Tables 1 and 2, respectively. Compared to patients with predominantly non-homogeneous neointima, those with a predominantly homogeneous one showed a higher prevalence of

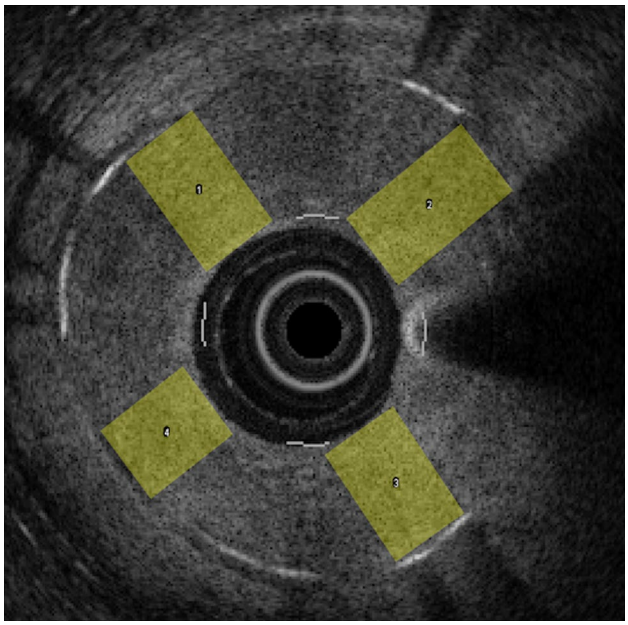

Fig. 2 Gray-scale signal intensity analysis. An OCT cross section converted to a gray-scale image with superimposed regions of interest in four different quadrants

diabetes mellitus (26.5% vs. 49.3%; $p=0.026$) and multivessel disease (52.9% vs. 72.6%; $p=0.045$) as well as a lower %DS [71.0% (64.0–81.0) vs. 60.9% (54.8–69.0); $p=0.001$]. The remaining clinical and angiographic characteristics were evenly distributed between groups.

Underlying stent type was a bare-metal stent (BMS) in 37 (34.6%), DES in 64 (59.8%), and bioresorbable vascular scaffold (BVS) in 6 (5.6%) patients. Further classification as a function of time from index stenting showed 47 patients (14 BMS, 28 DES and 5 BVS) presenting with early (< 1 year), 20 patients (1 BMS, 18 DES and 1 BVS) with late (1–3 years) and 40 patients (22 BMS and 18 DES) with very late (> 3 years) ISR.

OCT morphometric analysis

OCT morphometric data according to predominant neointimal type are reported in Table 3. Maximal %AS [73.8 (67.9–85.7) vs. 69.9 (60.1–78.9); $p=0.023$], maximal neointimal thickness [1090.0 (872.5–1235.0) vs. 950.0 (710.0–1090.0) µm; $p=0.008$], neointimal area [2.69 (1.48–4.52) vs. 2.13 (1.16–3.51) mm^2; $p=0.003$], mean SA [7.13 (5.96–8.43) vs. 6.09 (5.01–7.64) mm^2 ($p=0.007$)] as well as minimal SA [5.46 (4.52–6.36) vs. 4.61 (3.64–5.49) mm^2; $p=0.005$] were significantly higher in the non-homogeneous group. SEI was 0.73 (0.62–0.85) and 0.79

Table 1 Clinical characteristics of the patient population

	Predominantly non-homogeneous ($n=34$)	Predominantly homogeneous ($n=73$)	p value
Age	69.9 (58.1–76.6)	66.0 (58.1–74.9)	0.597
Women	8 (23.5)	9 (12.3)	0.140
Arterial hypertension	26 (76.5)	63 (86.3)	0.206
Hypercholesterolemia	23 (67.6)	59 (80.8)	0.134
Diabetes mellitus	9 (26.5)	36 (49.3)	0.026
Oral therapy	4 (11.8)	22 (30.1)	0.039
Insulin-dependent	2 (5.9)	10 (13.7)	0.331
Current smoker	3 (8.8)	10 (13.7)	0.545
Ex-smoker	13 (38.2)	35 (47.9)	0.347
Body mass index, kg/m^2	27.3 (23.8–29.8)	28.1 (25.9–31.2)	0.112
Clinical presentation			0.111
Stable angina	12 (35.3)	43 (58.9)	
Silent ischemia	5 (14.7)	6 (8.2)	
Unstable angina	9 (26.5)	14 (19.2)	
NSTEMI	7 (20.6)	10 (13.7)	
STEMI	1 (2.9)	0 (0.0)	
Acute coronary syndrome	17 (50.0)	24 (32.9)	0.089
Previous MI	22 (64.7)	44 (60.3)	0.661
Previous CABG	2 (5.9)	4 (5.5)	1.000
LVEF, %	60.0 (53.0–70.0)	60.0 (50.0–65.0)	0.363

Data are shown as numbers (%) or median (inter quartile range)

CABG coronary artery bypass grafting, *LVEF* left ventricular ejection fraction, *MI* myocardial infarction, *NSTEMI* non-ST-elevation myocardial infarction, *STEMI* ST-elevation myocardial infarction

Table 2 Angiographic characteristics of the patient population

	Predominantly non-homogeneous ($n=34$)	Predominantly homogeneous ($n=73$)	p value
Target vessel			0.620
Left main	1 (2.9)	0 (0.0)	
LAD	16 (47.1)	36 (49.3)	
LCx	7 (20.6)	15 (20.5)	
RCA	10 (29.4)	22 (30.1)	
Diseased vessels			0.134
One	16 (47.1)	20 (27.4)	
Two	6 (17.6)	17 (23.3)	
Three	12 (35.3)	36 (49.3)	
Multivessel disease	18 (52.9)	53 (72.6)	0.045
Restenosis morphology			0.208
Focal body	17 (50.0)	19 (26.0)	
Focal margin	4 (11.8)	14 (19.2)	
Diffuse intrastent	9 (26.5)	28 (38.4)	
Multifocal	1 (2.9)	3 (4.1)	
Proliferative	3 (8.8)	9 (12.3)	
QCA			
Lesion length (mm)	11.9 (7.4–18.4)	12.1 (8.7–19.1)	0.763
RVD (mm)	2.84 (2.49–3.13)	2.68 (2.43–2.93)	0.231
% DS	71.0 (64.0–81.0)	60.9 (54.8–69.0)	0.001
AHA/ACC lesion type			0.243
A	2 (5.9)	0 (0.0)	
B1	9 (26.5)	25 (34.2)	
B2	16 (47.1)	33 (45.2)	
C	7 (20.6)	15 (20.5)	
Ostial lesion	2 (5.9)	8 (10.9)	0.498
Bifurcation lesion	5 (14.7)	21 (28.8)	0.114
Index stent interval (days)	310 (240–1655)	550 (206–2702)	0.677
Early (< 1 year)	246 (201–289)	197 (179–268)	0.087
Late (1–3 years)	584 (494–678)	492 (403–759)	0.653
Very late (> 3 years)	4170 (2217–5243)	3276 (2017–3950)	0.267
Restenosis age			0.229
Early	19 (55.9)	28 (38.5)	
Late	4 (11.8)	16 (21.4)	
Very late	11 (32.4)	29 (40.1)	
Index stent type			0.323
BMS	12 (35.3)	25 (34.2)	
G1-DES	8 (23.5)	19 (26.0)	
G2-DES	14 (41.2)	23 (31.5)	
BVS	0 (0.0)	6 (8.2)	

Data are shown as numbers (%) or median (inter quartile range)

BMS bare-metal stent, *BVS* bioresorbable vascular scaffold, *DS* diameter stenosis, *G1-DES* first-generation drug-eluting stent, *G2-DES* second-generation drug-eluting stent, *LAD* left anterior descending artery, *LCx* left circumflex artery, *MLD* minimal lumen diameter, *%DS* percent diameter stenosis, *QCA* quantitative coronary analysis, *RCA* right coronary artery, *RVD* reference vessel diameter

(0.70–0.86) ($p=0.420$), with stent underexpansion being present in 16 (48.5%) and 44 (61.1%) lesions, respectively ($p=0.225$) (Fig. 3). The percentage of both uncovered [strut coverage 96.4% vs. 96.6%; $p=0.659$] and malapposed struts [0.74% vs. 0.55%; $p=0.776$] was extremely low in both groups. Additional comparisons between different stent platforms are reported in the Appendix in the online-only Data Supplement.

Table 3 Optical coherence tomography characteristics of the patient population

	Predominantly non-homogeneous ($n=34$)	Predominantly homogeneous ($n=73$)	p value
Stent length (mm)	26.0 (18.2–34.3)	25.6 (18.7–32.2)	0.763
Nr. of struts per lesion	146.0 (91.5–281.2)	216.0 (144.0–295.0)	0.118
Mean stent area (mm^2)	7.13 (5.96–8.43)	6.09 (5.01–7.64)	0.007
Min. stent area (mm^2)	5.46 (4.52–6.36)	4.61 (3.64–5.49)	0.005
Mean lumen area (mm^2)	4.25 (2.67–5.93)	3.55 (2.39–5.16)	0.325
Min. lumen area (mm^2)	1.69 (0.86–2.47)	1.66 (1.15–2.19)	0.715
Mean neointimal thickness (μm)	310.0 (150.0–570.0)	270.0 (140.0–490.0)	0.008
Maximal neointimal thickness (μm)	1090.0 (872.5–1235.0)	950.0 (710.0–1090.0)	0.008
Neointimal area (mm^2)	2.69 (1.48–4.52)	2.13 (1.16–3.51)	0.003
Strut coverage (%)	96.4	96.6	0.659
Strut malapposition (%)	0.74	0.55	0.776
Malapposition distance	160.0 (130.0–277.5)	160.0 (140.0–210.0)	0.079
Mean % area stenosis	39.6 (20.9–60.9)	37.8 (20.9–56.7)	0.078
Max. % area stenosis	73.8 (67.9–85.7)	69.9 (60.1–78.9)	0.023
Stent expansion index	0.73 (0.62–0.85)	0.79 (0.70–0.86)	0.420
Stent underexpansion	16 (48.5)	44 (61.1)	0.225

Data are shown as numbers (%) or median (inter quartile range)

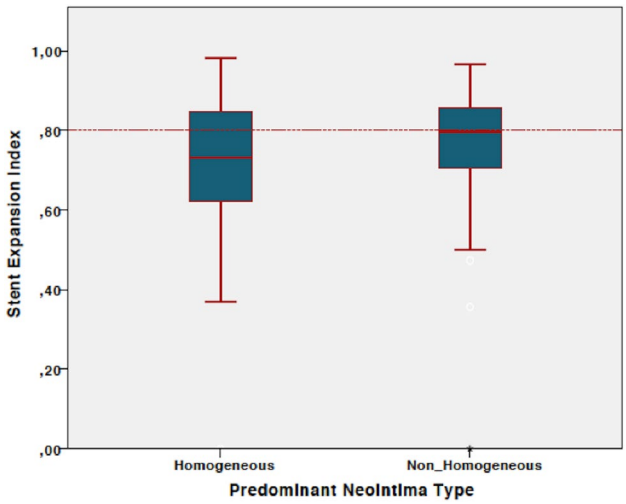

Fig. 3 Distribution of stent expansion index values according to predominant neointima type with stent underexpansion being defined by a stent expansion index < 0.80

Qualitative neointimal characterization and gray-scale signal intensity analysis

The qualitative analysis showed that predominantly homogeneous lesions included 4.5%(0.0–14.3) non-homogeneous quadrants, while predominantly non-homogeneous ones included 28.1%(20.3–37.5) homogeneous quadrants (Fig. 4a, b). There was excellent interobserver agreement regarding neointimal characterization (Cohen's $\kappa=0.931$).

GSI analysis was performed in a total of 3648 quadrants. Homogeneous quadrants were characterized by the highest mean GSI values [108.4 (92.5–123.6)], followed by those with NA [88.3 (72.8–104.9)], with non-homogeneous quadrants showing the lowest GSI values [79.9 (61.2–95.9)]. One-way ANOVA as well as pairwise comparisons by means of the Tukey post hoc test showed a statistically significant difference for each between group comparison ($p<0.001$ for all comparisons) (Fig. 5).

Neoatherosclerosis

The presence of any frame with NA was registered in 33 (30.8%) lesions. Neoatherosclerotic changes were present in 15 (40.5%) BMS and 18 (25.7%) DES lesions ($p=0.114$); the presence of any frame with NA was observed in 6 (12.8%) early, 6 (30.0%) late, and 21 (52.5%) very late lesions ($p<0.001$). When analyzing the presence of NA on the basis of both underlying stent type and time from index stenting, some clear differences emerge between BMS and DES (Fig. 6), with clustering of BMS NA in the very late phase and no evidence of such changes up to 3 years (0% early, 0% late, and 68.2% very late BMS lesions; $p<0.001$); on the contrary, DES lesions displayed an earlier appearance of NA (18.2% early, 31.6% late, and 33.3% very late DES lesions; $p=0.393$). Comparisons of neointimal characteristics and presence of NA between G1-DES and G2-DES are reported in the Appendix in the online-only Data Supplement.

Quantitative analysis of NA, expressed as percentage of quadrants with NA per lesion, was also

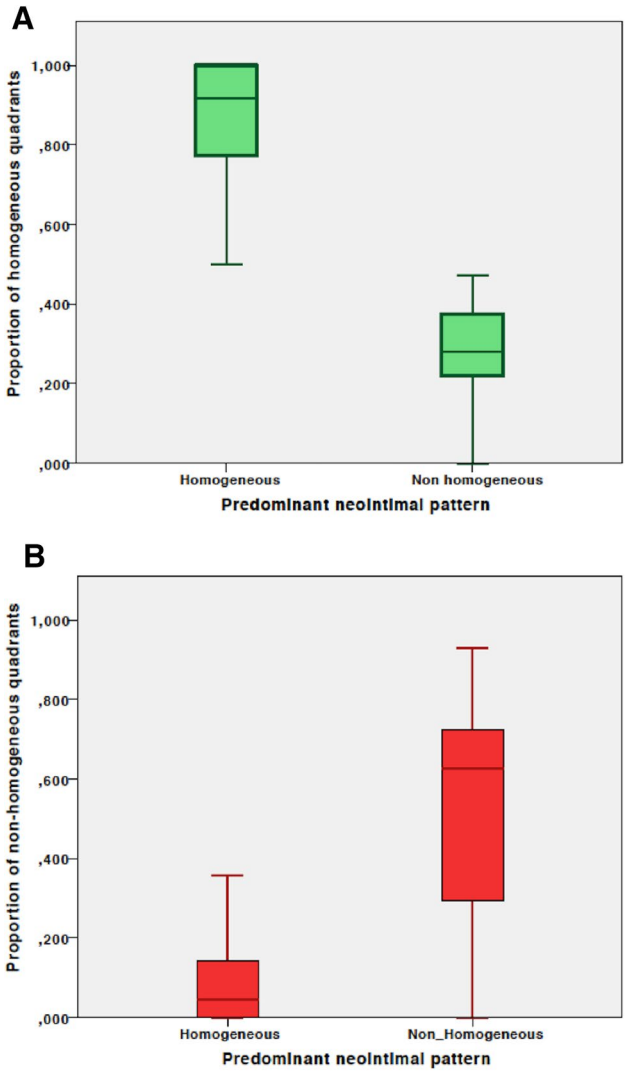

Fig. 4 Distribution of homogeneous and non-homogeneous quadrants according to predominant neointimal pattern of in-stent restenosis lesion. **a** Proportion of homogeneous quadrants according to predominant neointimal pattern. **b** Proportion of non-homogeneous quadrants according to predominant neointimal pattern

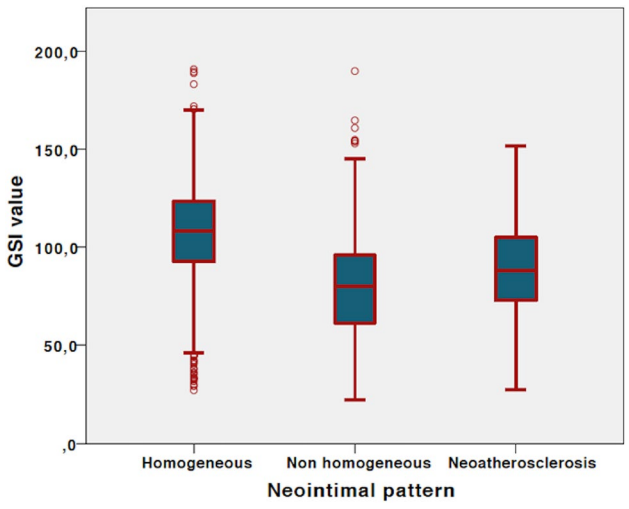

Fig. 5 Gray-scale signal intensity values for homogenous, non-homogeneous, and neoatherosclerosis quadrants

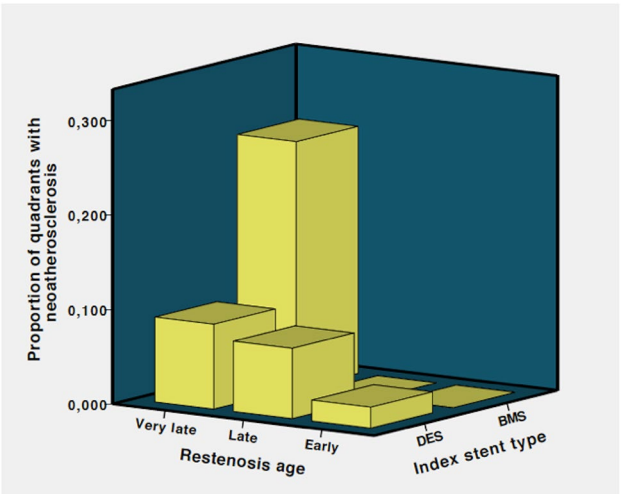

Fig. 6 Proportion of quadrants displaying neoatherosclerotic changes according to stent type and restenosis age

significantly different among BMS (15.6 ± 26.1%) and DES (5.4%±11.9%) ($p = 0.05$) as well as among early (1.6 ± 5.1%), late (7.1 ± 12.5%) and very late (18.4 ± 26.0%) lesions ($p < 0.001$). Finally, the percentage of quadrants with NA was significantly higher in the predominantly non-homogeneous group (20.0 ± 28.2% vs. 3.9 ± 8.5%; $p = 0.005$).

Predictors of OCT neointimal patterns and neoatherosclerosis

Multivariable analysis showed that female sex [odds ratio (OR) 3.67; 95% confidence interval (CI) 1.03–13.2; $p = 0.046$] and maximal neointimal thickness (OR for 1 mm increase 14.3; 95% CI 2.09–98.57; $p = 0.007$) independently correlate with a predominantly non-homogeneous pattern, while angiographic pattern (OR for diffuse vs. focal restenosis 0.24; 95% CI 0.008–0.73; $p = 0.011$) and diabetes mellitus (OR 0.34; 95% CI 0.11–0.98; $p = 0.046$) inversely correlate with such a pattern (Fig. 7a). Time from index stenting procedure (OR for 1 year increase: 1.25; 95% CI 1.09–1.42; $p = 0.001$) was the only independent predictor of any frame with NA (Fig. 7b).

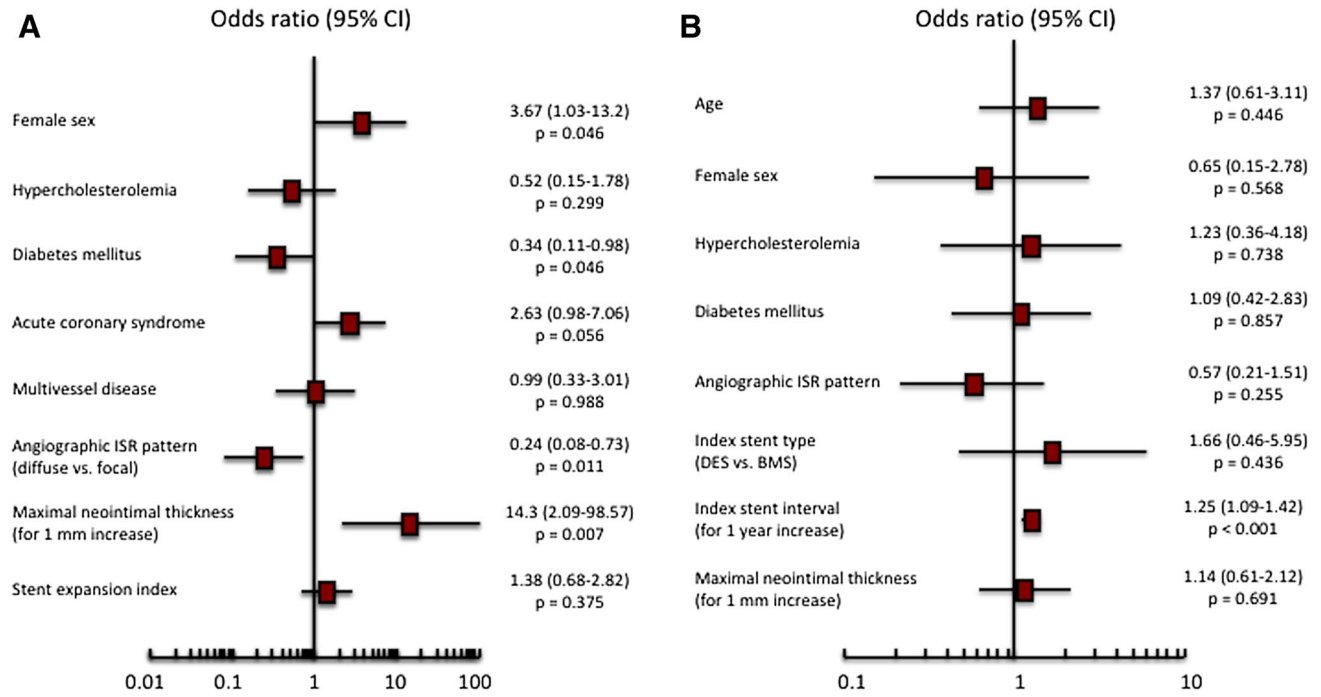

Fig. 7 Multivariable analysis for predictors of neointimal pattern as well as of neoatherosclerosis. Plot of odds ratios associated with non-homogeneous neointimal pattern (**a**) and with neoatherosclerosis (**b**). The squares indicate the point estimate and the left and right ends of the lines the 95% CI. *95%CI* 95% confidence interval, *ISR* in-stent restenosis, *BMS* bare-metal stent, *DES* drug-eluting stent

Discussion

Despite constant improvements in patient outcomes with modern stent platforms, ISR still occurs at not negligible rates. Given the two actually recommended strategies—repeat DES implantation vs. drug-coated balloon (DCB)—for the treatment of ISR [16, 17], the added value of OCT imaging could be represented by the identification of those lesions in which DCB angioplasty would guarantee optimal outcomes without additional stent implantation. To apply a histopathology-based [5] and treatment-oriented classification, we grouped the heterogeneous and layered patterns in one category.

The main findings of our study can be summarized as follows: (i) ISR lesions display considerable intralesion neointimal heterogeneity; (ii) female sex, diabetes mellitus, angiographic pattern of ISR, and maximal neointimal thickness independently correlate with neointimal pattern; (iii) GSI analysis shows that mean GSI values significantly differ between neointimal categories; (iv) NA is a not uncommon finding, develops earlier in DES compared to BMS and its presence and extent are time-dependent phenomena; and (v) the rate of stent underexpansion was high in both groups.

Since the majority of studies performed to date [9, 10, 18] categorized neointimal patterns based on the optical characteristics of a single frame, we expanded the analysis to include a 10 mm segment. We found that neointimal patterns different from the dominant one are significantly represented in the same restenotic lesion. Therefore, a detailed analysis of the neointimal characteristics of the whole stented segment seems advisable for proper classification of restenotic lesions [16, 18]. The impact of the presence and extent of neointimal heterogeneity on clinical and angiographic outcomes following treatment of ISR remains to be investigated in specifically designed studies.

The identification of maximal neointimal thickness as an independent correlate of non-homogeneous neointima deserves some further comments. Owing to progressive attenuation of the light beam, neointima of increasing thickness may display a reduced backscattering of the outermost layers and consequently a falsely non-homogeneous appearance; every care was taken to avoid such misclassification, as supported also by the extremely high interobserver agreement.

The classification of neointimal tissue has been a matter of debate and more reproducible strategies has been advocated [19]. Our analysis shows that mean GSI values significantly differ between neointimal categories. These results provide initial evidence on the usefulness of GSI analysis as a valuable quantitative adjunct in neointimal characterization. However, additional evaluation, ideally in the context of an OCT–histology correlation study, seems advisable to define the discriminatory capacity of GSI analysis. Analogously, whether more advanced quantitative

characterization, such as a combination of GSI with attenuation rate analysis [20], can further refine our ability to classify neointimal tissue remains to be determined.

NA has been involved in the pathogenesis of both ISR and stent thrombosis [21, 22]. Although NA was more frequent in BMS in absolute terms, this finding should be viewed in the light of significantly longer implant duration for BMS compared to DES [3347 (222.3–4308) vs. 389.5 (207.8–1302.8) days; $p = 0.005$]. Indeed, our findings support a strong time dependency of NA changes, with progressive increase in incidence with increasing time from stent implantation; indeed, time from index stenting was the only independent predictor of NA. Our results are in line with those of previous registries that showed duration of follow-up to be the most important risk factor for the occurrence of NA [12, 23]. A recent study by Song et al. also confirmed a higher incidence of NA in late as compared to early G2-DES ISR; besides time from index stenting, the absence of statin treatment and neointimal hyperplasia > 50% was identified as independent predictors of neoatherosclerosis [10]. The premature development of NA in DES compared to BMS is a noteworthy finding, since it closely mirrors findings of previous histopathological reports based on selected autopsy cases [24]; the proposed mechanism for such accelerated NA in DES involves delayed endothelialization and persistent endothelial dysfunction with consequent enhanced permeability of plasma lipoproteins [12]. These findings emphasize the importance of secondary prevention measures including risk factor control and intensive statin treatment.

Stent underexpansion has long been recognized as a major mechanical factor triggering ISR. In our patient collective, stent underexpansion was present in 48.5% and 61.1% of lesions, respectively. Despite differing definitions of stent underexpansion, our results are consistent with those reported in the study by Song et al. [10] and those of a more recent study by Miura et al. [25]. These findings have important therapeutic drawbacks, since recognition of stent underexpansion should prompt aggressive dilatation and eventually use of super-high-pressure non-compliant balloons. In addition, they underscore the importance of intravascular imaging guidance to optimize expansion during initial implantation as a mean to reduce the occurrence of ISR.

Study limitations

Some limitations should be considered when interpreting the results of the present report. First, the possible bias of patient selection should be considered, since the enrolment period spanned 5 years and patients presenting with ISR were not included consecutively; in addition, the study population is limited to patients who presented either with symptoms and/or with evidence of inducible myocardial ischemia. Second, this study is retrospective in nature, and therefore, its results should be interpreted as hypothesis generating. Third, since OCT imaging during index PCI was not performed, information regarding underlying plaque morphology is not available.

Conclusions

Neointimal patterns different from the dominant one are significantly represented in the same restenotic lesion. GSI analysis shows promise as a quantitative tool for neointimal characterization. Neoatherosclerothic changes are frequent in ISR lesions and show different time courses in DES as opposed to BMS and their presence and extent appear to be time-dependent phenomena.

Funding None.

Compliance with ethical standards

Conflict of interest The authors have no conflicts of interest to declare.

References

1. Cassese S, Byrne RA, Tada T, Pinieck S, Joner M, Ibrahim T, King LA, Fusaro M, Laugwitz KL, Kastrati A (2014) Incidence and predictors of restenosis after coronary stenting in 10 004 patients with surveillance angiography. Heart 100(2):153–159. https://doi.org/10.1136/heartjnl-2013-304933
2. Werner N, Nickenig G, Sinning JM (2018) Complex PCI procedures: challenges for the interventional cardiologist. Clin Res Cardiol 107(Suppl 2):64–73. https://doi.org/10.1007/s00392-018-1316-1
3. Gonzalo N, Serruys PW, Okamura T, van Beusekom HM, Garcia-Garcia HM, van Soest G, van der Giessen W, Regar E (2009) Optical coherence tomography patterns of stent restenosis. Am Heart J 158(2):284–293. https://doi.org/10.1016/j.ahj.2009.06.004
4. Kufner S, Xhepa E, Lutter C, Cassese S, Joner M (2017) Optical coherence tomography in drugeluting stent restenosis: a technique in need of a strategy. Minerva Cardioangiol 65(1):61–67. https://doi.org/10.23736/S0026-4725.16.04241-9
5. Lutter C, Mori H, Yahagi K, Ladich E, Joner M, Kutys R, Fowler D, Romero M, Narula J, Virmani R, Finn AV (2016) Histopathological differential diagnosis of optical coherence tomographic image interpretation after stenting. JACC Cardiovasc Interv 9(24):2511–2523. https://doi.org/10.1016/j.jcin.2016.09.016
6. Joner M, Finn AV, Farb A, Mont EK, Kolodgie FD, Ladich E, Kutys R, Skorija K, Gold HK, Virmani R (2006) Pathology of drug-eluting stents in humans: delayed healing and late thrombotic risk. J Am Coll Cardiol 48(1):193–202. https://doi.org/10.1016/j.jacc.2006.03.042
7. Nakano M, Otsuka F, Yahagi K, Sakakura K, Kutys R, Ladich ER, Finn AV, Kolodgie FD, Virmani R (2013) Human autopsy study of drug-eluting stents restenosis: histomorphological predictors and neointimal characteristics. Eur Heart J 34(42):3304–3313. https://doi.org/10.1093/eurheartj/eht241
8. Habara M, Terashima M, Nasu K, Kaneda H, Inoue K, Ito T, Kamikawa S, Kurita T, Tanaka N, Kimura M, Kinoshita Y,

Tsuchikane E, Matsuo H, Ueno K, Katoh O, Suzuki T (2011) Difference of tissue characteristics between early and very late restenosis lesions after bare-metal stent implantation: an optical coherence tomography study. Circ Cardiovasc Interv 4(3):232–238. https://doi.org/10.1161/CIRCINTERVENTIONS.110.959999

9. Goto K, Takebayashi H, Kihara Y, Hagikura A, Fujiwara Y, Kikuta Y, Sato K, Kodama S, Taniguchi M, Hiramatsu S, Haruta S (2013) Appearance of neointima according to stent type and restenotic phase: analysis by optical coherence tomography. EuroIntervention 9(5):601–607. https://doi.org/10.4244/EIJV9I5A96
10. Song L, Mintz GS, Yin D, Yamamoto MH, Chin CY, Matsumura M, Kirtane AJ, Parikh MA, Moses JW, Ali ZA, Shlofmitz RA, Maehara A (2017) Characteristics of early versus late in-stent restenosis in second-generation drug-eluting stents: an optical coherence tomography study. EuroIntervention. https://doi.org/10.4244/EIJ-D-16-00787
11. Mehran R, Dangas G, Abizaid AS, Mintz GS, Lansky AJ, Satler LF, Pichard AD, Kent KM, Stone GW, Leon MB (1999) Angiographic patterns of in-stent restenosis: classification and implications for long-term outcome. Circulation 100(18):1872–1878
12. Otsuka F, Byrne RA, Yahagi K, Mori H, Ladich E, Fowler DR, Kutys R, Xhepa E, Kastrati A, Virmani R, Joner M (2015) Neoatherosclerosis: overview of histopathologic findings and implications for intravascular imaging assessment. Eur Heart J 36(32):2147–2159. https://doi.org/10.1093/eurheartj/ehv205
13. Malle C, Tada T, Steigerwald K, Ughi GJ, Schuster T, Nakano M, Massberg S, Jehle J, Guagliumi G, Kastrati A, Virmani R, Byrne RA, Joner M (2013) Tissue characterization after drug-eluting stent implantation using optical coherence tomography. Arterioscler Thromb Vasc Biol 33(6):1376–1383. https://doi.org/10.1161/ATVBAHA.113.301227
14. Koppara T, Tada T, Xhepa E, Kufner S, Byrne RA, Ibrahim T, Laugwitz KL, Kastrati A, Joner M (2018) Randomised comparison of vascular response to biodegradable polymer sirolimus eluting and permanent polymer everolimus eluting stents: an optical coherence tomography study. Int J Cardiol 258:42–49. https://doi.org/10.1016/j.ijcard.2018.01.011
15. Tibshirani R (1997) The lasso method for variable selection in the Cox model. Stat Med 16(4):385–395
16. Alfonso F, Byrne RA, Rivero F, Kastrati A (2014) Current treatment of in-stent restenosis. J Am Coll Cardiol 63(24):2659–2673. https://doi.org/10.1016/j.jacc.2014.02.545
17. Colleran R, Kastrati A (2018) Percutaneous coronary intervention: balloons, stents and scaffolds. Clin Res Cardiol 107(Suppl 2):55–63. https://doi.org/10.1007/s00392-018-1328-x
18. Tada T, Kadota K, Hosogi S, Miyake K, Ohya M, Amano H, Izawa Y, Kanazawa T, Kubo S, Ichinohe T, Hyoudou Y, Hayakawa Y, Sabbah MM, Otsuru S, Hasegawa D, Habara S, Tanaka H, Fuku Y, Katoh H, Goto T, Mitsudo K (2015) Association between tissue characteristics assessed with optical coherence tomography and mid-term results after percutaneous coronary intervention for in-stent restenosis lesions: a comparison between balloon angioplasty, paclitaxel-coated balloon dilatation, and drug-eluting stent implantation. Eur Heart J Cardiovasc Imaging 16(10):1101–1111. https://doi.org/10.1093/ehjci/jev031
19. Sakakura K, Joner M, Virmani R (2014) Does neointimal characterization following DES implantation predict long-term outcomes? JACC Cardiovasc Imaging 7(8):796–798. https://doi.org/10.1016/j.jcmg.2014.06.002
20. Rheude TA, Xhepa E, Byrne RA (2017) Markedly different tissue types on optical coherence tomography imaging in a patient with multiple lesion drug-eluting stent in-stent restenosis. Catheter Cardiovasc Interv 89(6):E181–E184. https://doi.org/10.1002/ccd.26694
21. Adriaenssens T, Joner M, Godschalk TC, Malik N, Alfonso F, Xhepa E, De Cock D, Komukai K, Tada T, Cuesta J, Sirbu V, Feldman LJ, Neumann FJ, Goodall AH, Heestermans T, Buysschaert I, Hlinomaz O, Belmans A, Desmet W, Ten Berg JM, Gershlick AH, Massberg S, Kastrati A, Guagliumi G, Byrne RA (2017) Prevention of late stent thrombosis by an interdisciplinary global european effort. Optical coherence tomography findings in patients with coronary stent thrombosis: a report of the PRESTIGE consortium (prevention of late stent thrombosis by an interdisciplinary global european effort). Circulation 136(11):1007–1021. https://doi.org/10.1161/CIRCULATIONAHA.117.026788
22. Alfonso F, Fernandez-Vina F, Medina M, Hernandez R (2013) Neoatherosclerosis: the missing link between very late stent thrombosis and very late in-stent restenosis. J Am Coll Cardiol 61(12):e155. https://doi.org/10.1016/j.jacc.2012.09.071
23. Otsuka F, Vorpahl M, Nakano M, Foerst J, Newell JB, Sakakura K, Kutys R, Ladich E, Finn AV, Kolodgie FD, Virmani R (2014) Pathology of second-generation everolimus-eluting stents versus first-generation sirolimus- and paclitaxel-eluting stents in humans. Circulation 129(2):211–223. https://doi.org/10.1161/CIRCULATIONAHA.113.001790
24. Nakazawa G, Otsuka F, Nakano M, Vorpahl M, Yazdani SK, Ladich E, Kolodgie FD, Finn AV, Virmani R (2011) The pathology of neoatherosclerosis in human coronary implants bare-metal and drug-eluting stents. J Am Coll Cardiol 57(11):1314–1322. https://doi.org/10.1016/j.jacc.2011.01.011
25. Miura K, Tada T, Habara S, Kuwayama A, Shimada T, Ohya M, Murai R, Amano H, Kubo S, Otsuru S, Tanaka H, Fuku Y, Goto T, Kadota K (2018) Optical coherence tomography predictors for recurrent restenosis after paclitaxel-coated balloon angioplasty for drug-eluting stent restenosis. Circ J. https://doi.org/10.1253/circj.CJ-18-0464